

© 2016 Optical Society of America. One print or electronic copy may be made for personal use only. Systematic reproduction and distribution, duplication of any material in this paper for a fee or for commercial purposes, or modifications of the content of this paper are prohibited.

# Pupil filters for extending the field-of-view in light-sheet microscopy

DEAN WILDING<sup>1,\*</sup>, PAOLO POZZI<sup>1</sup>, OLEG SOLOVIEV<sup>1,3</sup>, GLEB VDOVIN<sup>1,3</sup>, COLIN J. SHEPPARD<sup>2</sup>, AND MICHEL VERHAEGEN<sup>1</sup>

<sup>1</sup>Delft Center for Systems and Control, Delft University of Technology, Mekelweg 2, 2628 CD Delft, The Netherlands

<sup>2</sup>Italian Institute of Technology, Genova, Italy

<sup>3</sup>Flexible Optical B.V, Rijswijk, the Netherlands

\* Corresponding author: d.wilding@tudelft.nl

Compiled January 8, 2016

**Pupil filters, represented by binary phase modulation, have been applied to extend the field of view of a light-sheet fluorescence microscope. Optimization has been used first numerically to calculate the optimum filter structure, and then experimentally, to scale and align the numerically synthesized filter in the microscope. A significant practical extension of the field of view has been observed, making reported approach a valuable tool on a path to wide-field light-sheet microscopy.** ©

2016 Optical Society of America

**OCIS codes:** (180.0180) Microscopy; (180.2520) Fluorescence microscopy; (180.6900) Three-dimensional microscopy; (220.1080) Active or adaptive optics; (050.1220) Apertures; (050.1380) Binary optics

<http://dx.doi.org/10.1364/ao.XX.XXXXXX>

Light-sheet (LS) microscopy [1, 2] achieves optical sectioning in specimens by forming a thin LS in the plane orthogonal to the optical axis of an imaging microscope. An ideal LS should be very thin, as the thickness of the LS defines the axial resolution. As an additional requirement the thickness and intensity of the LS should both be kept as uniform as possible over the field-of-view (FOV). The LS should be wide and long enough to cover the whole FOV of the microscope.

In practice, however, the parameters of the LS are governed by laws of diffraction and scattering in the specimen, and therefore, the ideal parameters are hardly ever achieved. The optimization of these parameters for a LS is of interest for a number of practical applications in biomedical imaging [3]. There has been much work done on the enhancement of the LS, this includes the creation of scanned Bessel beams [4], Airy beams [5], and aspheric optical systems [6].

In all such approaches the goal is a redistribution of the light field that enables the light to propagate with a lower divergency in the vicinity of the focus. The theoretically optimum solution in three-dimensions is the infinite energy Bessel beam [7], and its two-dimensional equivalent the cosine beam [8]. In practice, the Bessel beam cannot be produced; however, hybrids of these beams with the Gaussian beam can be obtained [9]. The

weakness of all of these beam engineering techniques are the strengthening of the subsidiary side lobes that decrease the optical sectioning ability in the LS microscope; this can be reduced by deconvolution post-processing [5], but it still remains a limiting factor.

It was shown by Shepherd in [10] that a symmetric binary pupil filter (PF) can be used for maximizing the extension of a two-dimensional LS formed by a cylindrical lens with a band structure of  $0 \vee \pi$  phase shifts. The band positions are symmetrical with respect to the optical axis of the lens, but have no rotational symmetry.

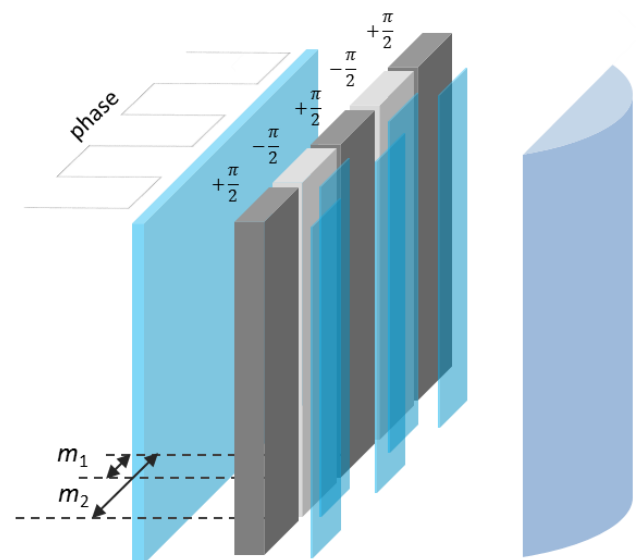


**Fig. 1.** A schematic showing the realization of pupil filters in a LS microscope. The field is modulated by the introduction of  $\pi$  phase differences before a cylindrical phase element in the pupil. By controlling the shape of the band structure the focal intensity distribution is changed.

The PF solutions could theoretically out-perform the Gauss-Bessel beams [10], therefore, is calling for experimental verification. The generalization of this technique to complex pupil

functions could allow for the additional correction and compensation of aberrations introduced by the sample and is an active area of our research. Since our hope is to show that PFs can provide an alternative to expensive adaptive elements we have limited our scope.

In Figure 1 the structure of the PF is shown alongside the cylindrical element that forms the LS. The PF considered in this letter have  $N$  symmetric elements with  $M = (N - 1)/2$  step changes in the phase as the half-aperture is traversed. Following the same notation as in [10], these parameters are called  $m_i$ 's,  $i = 1, \dots, M$ , the normalized pupil coordinates at which the step change occurs.

For clarity of explanation Figure 2 shows the schematic of the geometric of the LS microscope system. The orthogonal detection of the light in the illumination path and the fluorescence path are shown. The coordinate system represented in the Figure is used throughout the text.

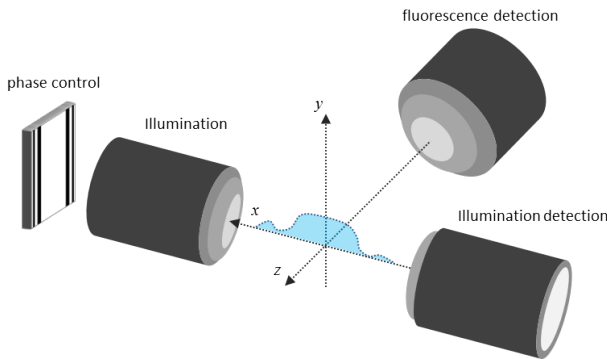


**Fig. 2.** The axes configuration in the focal plane for the detection of illumination light and fluorescence light. The light enters from the left via the phase element and is focused along the  $xy$ -plane. Depth is with respect to the fluorescence objective.

The solutions to the wave equation for elements up to  $N = 7$  are presented in Table 1 of [10]; however, to find the solutions for  $N > 7$  requires an ever increasing amount of time by brute force. Hence it is highly desirable to find the solutions via more time efficient numerical optimization techniques. Moreover, in order to implement these PFs on the experimental system it is necessary to calibrate the  $m_i$ 's to further improve the parameters of LS.

Optimization is finding the minimum of a cost or objective function that represents a physical measure as functions of decision variables. Concretely, in [10] a parameter  $G_A$  is proposed with its decision variables  $m_i$ 's. It is a measure of the axial point-spread function and is derived from the analysis of the pupil field moments, however, it is impossible to apply this metric to the experimental setup.

To overcome this, a new metric, one that can be experimentally measured is proposed in this letter. Measurements of the focal field are taken at  $K$  positions along the optical axis giving peak intensities  $I_k$ . Typically, it was found that  $K = \mathcal{O}(M)$  is sufficient. The root mean square deviation from the maximum focal intensity is then calculated:

$$\text{r.m.s.} = \rho = \sqrt{\frac{1}{K} \sum_{k=0}^K (I_k - \max(I_k))^2} \quad (1)$$

The PF solution that provides good LS parameters forms a flat intensity profile around the focus along the optical axis. This implies the curvature of the intensity field is minimized, i.e.  $G_A \rightarrow 0$ . Therefore, the optimal PF solution,  $\mathbf{m}^*$ , that minimizes the deviation from peak intensity,  $\rho$ , over a given range  $\Delta$  is what is desired.

The problem can be written as,

$$\begin{aligned} \min_{\mathbf{m}} \quad & \rho(\mathbf{m}, \Delta) \\ \text{s.t.} \quad & m_i + \delta < m_{i+1} \end{aligned} \quad (2)$$

where  $\mathbf{m} \in \mathbb{R}^{(N-1)/2}$  are the optimization variables.  $\delta$  is the width of a Fresnel zone in the pupil. Although modest in dimension for a small number of elements, the problem is not trivial to solve. The objective function is non-convex and has a number of local minima, although, it is a simpler problem than the minimization of  $G_A$  due to the numerical instability of the metric. Furthermore, as the number of dimensions is expanded, the number of non-optimal local minimizers increases.

These local minima arise due to the complex interference interactions between different regions in the pupil. For example, it is possible for the positioning of two of the zones to provide a net effect of zero to the field. Hereby, the numerical procedure for example can find the  $N = 3$  solution in all higher dimensions with increasing permutations. For this reason the value of  $\Delta$  becomes a very important tuning parameter in the optimization, too high and the solution will not exist and too low the number of non-global minima increases slowing the process.

The global optimization is performed with a custom algorithm written by the authors that uses a stochastic gradient descent [11] to converge to multiple minima simultaneously. Each group of solutions is evaluated on the strength of the group's weighted mean or centroid rather than the individuals to increase robustness against noise.

In Figure 3 the  $x$ -profiles for the PF solutions for  $N = 1, 3, \dots, 11$  found in the simulated environment are shown. The simulated fields are obtained with Fresnel propagation within the approximations of scalar diffraction theory [12]. The main result shown is that increasing the value of  $N$  increases the axial extend of the PSF, likewise, it increases the lateral extent also but less than simply increasing the numerical aperture (NA). This was shown in [10] for  $N = 3, \dots, 7$  and it has been extended to  $N = 11$  here.

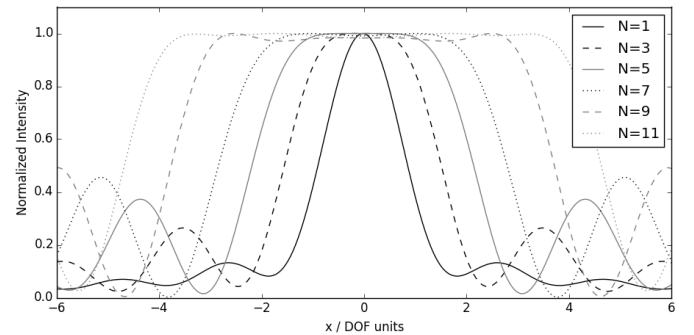


**Fig. 3.** Simulations of the intensity profile along the  $x$ -axis. Increasing the number of elements in the pupil filter increases the axial extend of the PSF and therefore, increases the uniformity over the FOV in a LS microscope. The intensity is normalized in this plot.

The problem is more complicated experimentally due to the noise introduced in the intensity measurements, therefore, it was impossible to consistently find the solution to the global optimization on the experimental setup.

To overcome this a two-stage optimization process was required to consistently find the solution. Firstly, the global optimum is found via simulation with the advantage of no measurement noise. Secondly, this solution is locally optimized on the experimental system to correct for pupil matching, system aberrations and differences in magnification.

This can be done since in a region close to the theoretical global minimum the cost function is quasi-convex. The local optimization can proceed using a noise robust algorithm [13]. This process converges to the new minimum within a few iterations, typically under 25. Here the pupil phase,  $\phi(\mathbf{m})$  is optimized with  $\mathbf{c} \in \mathbb{R}^2$  such that the new phase  $\phi'(\mathbf{m})$  is:

$$\phi'(\mathbf{m}) = c_0\phi(c_1\mathbf{m}) \quad (3)$$

The LS microscope has been realized with a liquid crystal phase-only spatial light modulator (SLM) (512x512, Meadowlark/Boulder, US) conjugated to the pupil of a NA= 0.3 water immersion illumination objective (UMPLFLN 10x Olympus, Japan). Such a configuration allows for the forming arbitrary pupil functions with high resolution; however, in this letter the scope of possible solutions are limited to the class described in [10].

A 488nm laser source (100mW Sapphire 488nm LP, Coherent, US) illuminates the PF generated by the SLM and is conjugated with the pupil plane of the illumination objective mounted in a custom water immersion sample chamber. The measurements of the objective function are obtained through a confocal objective (UMPLFLN 10x Olympus, Japan) onto CMOS camera (DCC1545M, Thorlabs, US). This is done at different values of defocus by modulating the phase on the SLM. A full intensity profile can also be imaged in the same manner by sweeping through a volume.

In Figure 4 the  $x$ -axis profile of the intensity for the optimized experimental PFs are shown for  $N = 1, \dots, 11$ . A good match between the theoretical prediction in Figure 3 and the experimental results is found, thus confirming the validity of the PF theory and its practical usefulness.

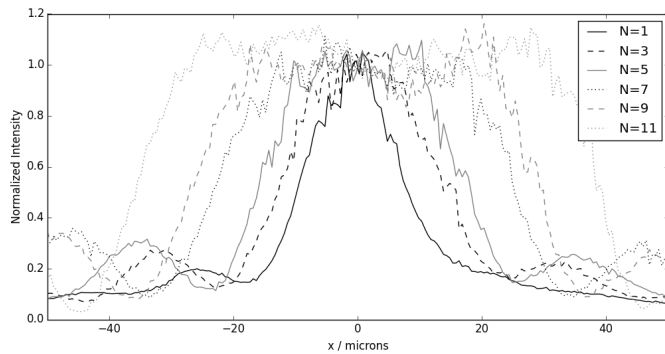


**Fig. 4.** Experimental plots of the intensity profile along the  $x$ -axis. In agreement with the simulations increasing the number of elements in the pupil filter increases the axial extend of the PSF. The plots are normalized to the mean intensity in a  $5\mu\text{m}$  central region.

Increasing the number of elements in the BFP increases the depth-of-field (DOF) whilst decreasing the focal intensity. For

discussion, in Figure 5 the  $xz$ -intensity of the  $N = 11$  optimized filter shown alongside the Gaussian beam and the numerical solution directly applied.

The first point to note is the improvement gained by the optimization procedure in the uniformity of the beam over the region. The numerical solution does not have the long uniform region over the FOV, but falls off after the focus, however, this is recovered by the optimization process. The PF must be matched to the pupil scale and the wavelength to gain optimal performance. The optimization ensures that both of these conditions are satisfied by scaling in size and amplitude. The  $\pi$  phase difference ensures a real pupil function giving the symmetry in the  $yz$ -plane seen in the optimized solution but which is missing in the unoptimized solution.

Measuring the full-width at half maximum (FWHM) for the  $N = 11$  filter shows a 4.2x increase in the DOF for a 1.6x increase in lateral PSF width. This is a better ratio than decreasing the NA 2.6x, and thus DOF extension has been achieved. In addition to this, the intensity is uniform over the central region, something that cannot be said about Gaussian or Gauss-Cosine beams. As a result there is a region of  $70\mu\text{m}$  that has a uniform intensity LS, this should in theory provide over this region better imaging than these other beam profiles.

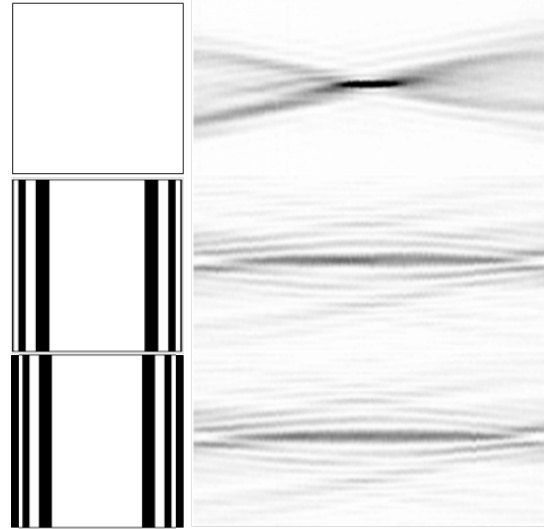


**Fig. 5.** Image of  $xz$  beam intensity profile produced by the illustrative PFs on the left. From the top the Gaussian, the numerical solution solution for  $N = 11$  and the optimized solution for  $N = 11$ . The region displaced for each PSF is  $100 \times 18\mu\text{m}$ . There is no normalization of intensity.

To further test this hypothesis, experimental investigation of the performance of the PF enhanced LS has been conducted by acquiring three dimensional volumes of fluorescent microspheres. The purpose is to measure the resolution of the microscope across the FOV. The axial PSF of the beads over the FOV varies according to the thickness of the LS at that position. The PFs designed to increase the LS extent whilst retaining lateral thickness is expected to improve the axial resolution towards the edges of the FOV.

The fluorescence image of the microsphere sample is captured via a relay system and a deformable mirror (DM69, Alpao, France) for focus change and detection, to scientific CMOS camera (Orca Flash 4, Hamamatsu Photonics, Japan). This configuration allows for full control of the LS and image focus for

three-dimensional imaging and sectioning of the sample.

In order to obtain sufficient sampling the  $z$ -scan is done using the DM in conjunction with the SLM. The system is calibrated such that plane of the LS and the focal plane of the detection objective are matched. The calibration procedure uses a sharpness-based optimization [14] to find the optimum defocus position at two known LS positions and form a linear model valid over the range of the defocus. Hereafter the focus of the detection objective and the LS remain coplanar.

The beam is scanned through a volume of the sample to produce a series of optically sectioned  $xy$  images at different  $z$  positions. This three-dimensional dataset can then be computationally processed and viewed from arbitrary angles, of which the orthogonal set  $xz$  is chosen. In Figure 6 the maximum intensity projections over small a  $y$ -range is shown for the  $N = 11$  optimized beam, along with the Gaussian and for reference a Gauss-Cosine beam.

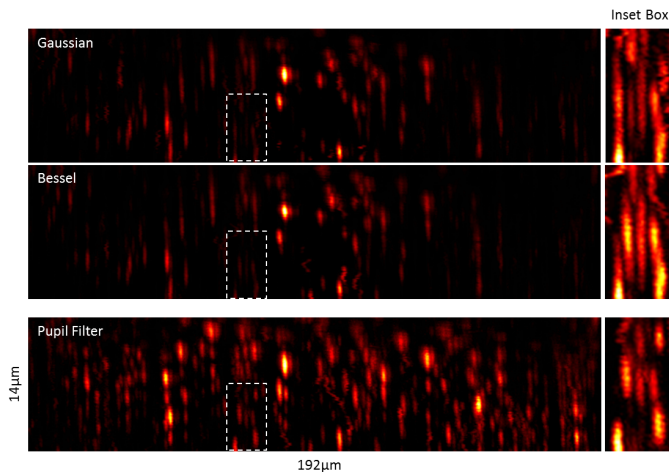


**Fig. 6.** Microspheres  $xz$ -profile with a Gaussian beam, a Bessel beam, and a PF  $N = 11$ . Same imaging parameters. The inset shows a zoom of beads at a distance of  $25\mu$  from the focus of the light-sheet.

This series of images show that the PF increases the uniformity of the resolution and intensity over the extension region compared with the Gaussian and Gauss-Cosine beam as expected. Outside of the  $50\mu\text{m}$  central region double and triple PSFs are observed consistent with the intensity profile shown in Figure 5.

The image contrast and the resolution in the center is decreased as a natural consequence of the extension of the DOF. The peak power decreases as  $N$  is increased such that the peak intensity for  $N = 11$  is a third of the original Gaussian power. The reason for this is both the lateral spreading of the PSF and redistribution of spatial frequencies, that is greater energy in side-lobes. The power in the center is decreased but the variance of the intensity across the FOV is minimized.

Binary pupil filters, therefore, are a simple and cost effective solution to the extension of the useful FOV in a LS microscope. The computation of the PF that provides a LS with optimal parameters is possible for large number of elements via numerical optimization. This allows for the design of filters with a long flat focus and therefore, a wide FOV for the LS microscope. Whilst it is possible, if not time consuming, to calculate the solutions for greater values of  $N$  at some point the reduction in peak power and increasing power in the side-lobes reduces the usefulness the PFs for imaging.

It has been shown how these PFs are found by a two stage process of numerical optimization, one to find the global solution via simulation and the second to find the local improvement on an experimental system. The profiles of the light intensity and their effect on the resolution of the microscope has been demonstrated.

It has been shown that the PFs produce a symmetric PSF along two axes owing to the real pupil function. This particular feature of PFs is not found in many other DOF extension methods such as the Gauss-Bessel beam or the Airy beam. It should be possible to exploit this symmetry to reduce the complexity in deconvolution calculations commonly employed in LS microscopy.

Finally, the PFs' theoretical advantage over the Gauss-Cosine or Gauss-Bessel beam has been shown experimentally, and since they do not require annuli for generation, more power can be delivered to the sample with the same source. Moreover, PFs could be manufactured as phase masks designed to fit particular microscope objectives. As a result the extended FOV could be realized with a much simpler, cheaper and durable system than presently available.

## ACKNOWLEDGMENTS

This work is sponsored by the European Research Council, Advanced Grant Agreement No. 339681. The authors would like to thank the contributions of R. Doelman, W.J.M. van Geest and C.J. Slinkman.

## REFERENCES

1. A. Voie, D. Burns, and F. Spelman, "Orthogonal-plane fluorescence optical sectioning: Three-dimensional imaging of macroscopic biological specimens," *Journal of microscopy* **170**, 229–236 (1993).
2. J. Huisken, J. Swoger, F. Del Bene, J. Wittbrodt, and E. H. Stelzer, "Optical sectioning deep inside live embryos by selective plane illumination microscopy," *Science* **305**, 1007–1009 (2004).
3. P. A. Santi, "Light sheet fluorescence microscopy a review," *Journal of Histochemistry & Cytochemistry* **59**, 129–138 (2011).
4. T. A. Planchon, L. Gao, D. E. Milkie, M. W. Davidson, J. A. Galbraith, C. G. Galbraith, and E. Betzig, "Rapid three-dimensional isotropic imaging of living cells using bessel beam plane illumination," *Nature methods* **8**, 417–423 (2011).
5. T. Vettenburg, H. I. Dalgarno, J. Nytk, C. Coll-Lladó, D. E. Ferrier, T. Čížmár, F. J. Gunn-Moore, and K. Dholakia, "Light-sheet microscopy using an airy beam," *Nature methods* **11**, 541–544 (2014).
6. S. Saghafi, K. Becker, C. Hahn, and H.-U. Dodt, "3d-ultramicroscopy utilizing aspheric optics," *Journal of biophotonics* **7**, 117–125 (2014).
7. J. Durnin, J. Miceli Jr, and J. Eberly, "Diffraction-free beams," *Physical Review Letters* **58**, 1499 (1987).
8. L. W. Casperson, D. G. Hall, and A. A. Tovar, "Sinusoidal-gaussian beams in complex optical systems," *JOSA A* **14**, 3341–3348 (1997).
9. C. Sheppard and T. Wilson, "Gaussian-beam theory of lenses with annular aperture," *IEE Journal on Microwaves, Optics and Acoustics* **2**, 105–112 (1978).
10. C. J. Sheppard, "Pupil filters for generation of light sheets," *Optics express* **21**, 6339–6345 (2013).
11. P. Wolfe, "Convergence conditions for ascent methods," *SIAM review* **11**, 226–235 (1969).
12. J. W. Goodman, *Introduction to Fourier optics* (Roberts and Company Publishers, 2005).
13. H. R. G. W. Verstraete, S. Wahls, J. Kalkman, and M. Verhaegen, "Model-based sensor-less wavefront aberration correction in optical coherence tomography," *Optics Letters* (2015).
14. R. A. Muller and A. Buffington, "Real-time correction of atmospherically degraded telescope images through image sharpening," *JOSA* **64**, 1200–1210 (1974).